Resolution limit of a phononic crystal superlens

J.-F. Robillard,[1,*] J. Bucay,[1] P. A. Deymier,[1] A. Shelke,[1] K. Muralidharan,[1] B. Merheb,[1] J. O. Vasseur,[2]
A. Sukhovich,[3,†] and J. H. Page[3]

[1]*Department of Materials Science and Engineering, University of Arizona, Tucson Arizona 85721, USA*

[2]*Institut d'Electronique, de Micro-électronique et de Nanotechnologie, UMR CNRS 8520, Cité Scientifique
F-59652 Villeneuve d'Ascq Cedex, France*

[3]*Department of Physics and Astronomy, University of Manitoba, Winnipeg, Manitoba, Canada R3T 2N2*

We report on the subwavelength imaging capabilities of a phononic crystal (PC) flat lens consisting of a triangular array of steel cylinders in methanol, all surrounded by water. The image resolution of the PC flat lens beats the Rayleigh diffraction limit because bound modes in the lens can be excited by evanescent waves emitted by the source. These are modes that only propagate in the direction parallel to the water-lens interface. These modes resonantly amplify evanescent waves that contribute to the reconstruction of an image. By employing the finite difference time domain method and ultrasonic experiments, we also explore the effect on the image resolution and focal point on various structural and operational parameters, such as source frequency, geometry of the lens, source position, and time. The mechanisms by which these factors affect resolution are discussed in terms of the competition between the contribution of propagative modes to focusing and the ability of the source to excite bound modes of the PC lens.

I. INTRODUCTION

Subwavelength resolution imaging has been a topic of considerable interest over the past decade. This effect is based on the ability of a system to transmit and focus the entire spatial Fourier spectrum from a source, including components which are nonpropagative. It was first demonstrated by Pendry[1] that focusing of electromagnetic waves could be achieved using a flat lens, in which incident waves undergo negative refraction. The concept of negative refraction also applies to acoustic waves.[2] enabling the development of negative index materials. Negative refraction can arise from one of two mechanisms. Systems can either consist of locally resonant structures, which exhibit a negative effective mass and negative bulk modulus,[2,3] or by a phononic crystal (PC), consisting of a periodic array of inclusions in a physically dissimilar matrix.[4–9] In the latter case, Bragg scattering leads to dispersive behavior with some pass bands exhibiting a negative group velocity. Bands with a negative group velocity lead to negative refraction. By employing PC flat lenses to focus acoustic waves, subwavelength imaging has been very recently demonstrated both experimentally and theoretically by Sukhovich and co-workers.[8,9] The authors reported subwavelength imaging of acoustic waves using a structure consisting of a triangular lattice of steel cylinders in methanol, all surrounded by water. In Ref. 9, PC lens super-resolution (resolution better than the diffraction limit of half the wavelength) was observed for the first time. Following this report, subwavelength imaging of acoustic waves has also been shown to be possible using a square lattice of inclusions on which a surface modulation is introduced,[10] a steel slab with a periodic array of slits,[11] and an acoustic hyperlens made from brass fins.[12] In these demonstrations, the mechanism by which this phenomenon occurs has been attributed to amplification of evanescent modes through bound surface or slab modes of the system. This allows for evanescent components to contribute to the reconstruction of the image. In studying the resolution of

photonic crystals, Luo *et al.*[13] developed an estimate for the maximum resolution achievable for a photonic crystal superlens.

In this paper we report a thorough study of the operational and geometrical factors affecting subwavelength imaging by a phononic crystal flat lens. We examine the relationship between geometrical factors and the band structure of the lens, with special attention paid to bound modes that lead to super-resolution. The paper is organized in the following manner: Sec. II provides a full description of the PC system as well as the computational and experimental methods used in calculations. We then provide, in Sec. III, an analytic interpretation of imaging with a homogeneous superlens system using a Green's function formalism that serves as a guide to understand the contributions of propagative and bound modes to the reconstruction of images. We then modify Luo's method,[13] in order to predict the resolution limit of a general flat lens, in Sec. IV. We apply this method to our PC and obtain a maximum resolution very close to that reported in Sec. II. In Sec. V, we demonstrate and analyze various operational and geometrical factors affecting the resolution of the PC flat lens as well as the focus location. These results are found to be in very good agreement with complementary experimental results. Finally, conclusions are drawn in Sec. VI regarding the relationship between geometry, nature of excitations, operating frequency, and resolution in PC flat lenses.

II. PHONONIC CRYSTAL SUPERLENS

A. Finite difference time domain simulation method

The system studied is similar to that of Sukhovich *et al.*[9] It consists of a PC slab immersed on all sides in water [Fig. 1(a)]. The PC is made of a triangular array of cylindrical steel inclusions in methanol. The radius of the inclusions is $r = 0.51$ mm with a lattice parameter of $a = 1.27$ mm. As explained in Ref. 8, methanol was selected as the fluid medium
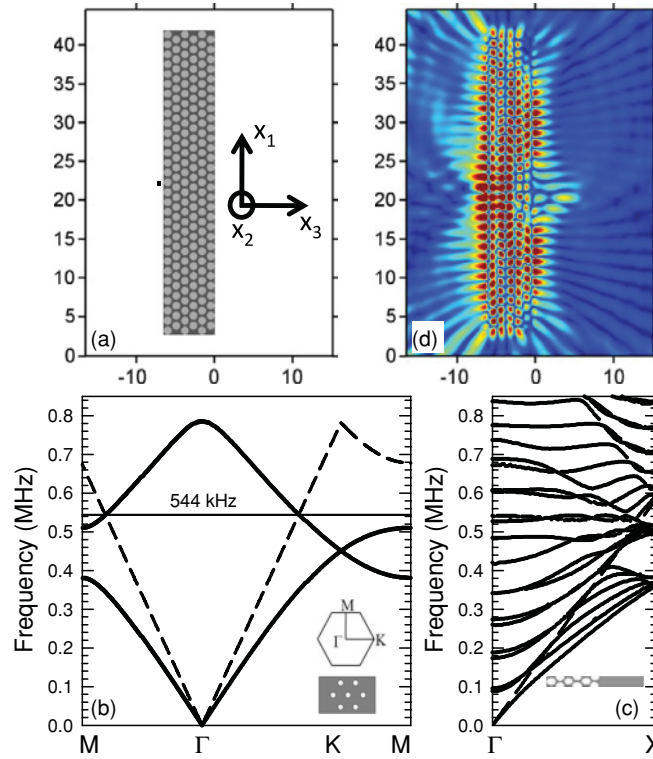
FIG. 1. (Color online) (a) The "standard configuration" phononic crystal system consisting of a triangular lattice of steel cylinders (light gray) in a methanol matrix (dark gray), all surrounded by water (white). The short, thick line located close to the center of the left side of the crystal represents the sound source. (b) FDTD dispersion curves of the infinite crystal (solid lines). The dashed line represents the dispersion curve in water. The intersection of the water cone with a negative group velocity band determines the frequency that results in a negative effective index of −1 for the PC. The inset shows the triangular crystal lattice of the PC with the corresponding unit cell and the contour of the first Brillouin zone. (c) FDTD band structure in the ΓX direction (parallel to the surface) for a finite six-layer crystal. Modes above water line correspond to propagating modes, while those which fall below are modes bound to the PC slab, which exhibit evanescent character. The inset depicts the supercell used in the calculation. (d) FDTD calculation of the average of the absolute value of the pressure over one period. On the exiting (right) side of the PC, an image is formed in the center accompanied by pressure lobes that decrease in magnitude as the distance from the surface of the crystal increases.

surrounding the steel rods in the PC so that, at a frequency in the second band, the size of the circular equifrequency contours of the crystal could be tuned to match the equifrequency contours of water outside the crystal. Thus one of the important conditions for good focusing could be achieved with this combination of materials. Indeed, any liquid with a sound velocity that is small enough relative to water would have sufficed, with methanol being a convenient choice not only because it is a low-loss fluid with a low velocity (approximately two-thirds the velocity in water) but also because it is readily available.

A finite difference time domain (FDTD) simulation method is employed to analyze propagation of acoustic waves through the PC lenses and the subsequent focusing upon exit of the crystal. The FDTD method is also used to calculate the band structure of the infinite PC and the finite PC lens systems. The FDTD method is based on a discretization of the equations of propagation of elastic waves in an inhomogeneous medium. Discretization of these equations is performed in the time and space domains on a square grid. It has been proven to be an efficient tool for calculating band structures as well as for studying wave propagation in PCs.[14–17] For further details on the description of this method, we refer the reader

to Sigalas *et al.*,[18] where the fully discretized equations are presented. All simulations used a spatial discretization of $dx = dy = 2 \times 10^{-5}$ m and a time step $dt = 6.09 \times 10^{-10}$ s to ensure convergence of results, as well as stability as imposed by the Courant condition. On all four sides of the simulation cell, Mur absorbing boundary conditions were used to avoid reflections.[19] We have verified that absorption conditions are not affected by the amount of water between the lens and the boundaries, provided that this distance is at least $2a$. The material parameters used are $\rho = 7890\,\text{kg/m}^3$, $c_t = 3100\,\text{m/s}$, and $c_l = 5800$ m/s for steel, $\rho = 790$ kg/m³, $c_t = 0$ m/s, and $c_l = 1138$ m/s for methanol, and $\rho = 1000$ kg/m³, $c_t = 0$ m/s, and $c_l = 1490$ m/s for water.

The FDTD band structure of the infinitely periodic PC in the principal symmetry directions of the Brillouin zone (BZ) is shown in Fig. 1(b). The inset depicts the triangular crystal structure geometry of the PC as well as the unit cell, in which the first Brillouin zone is shown. For this calculation, the structure is taken to be infinite in both directions by imposing periodic boundary conditions. The simulation time ($t = 2^{20} \times dt$) defines the error of the calculated frequencies to be $1/t = 1.6$ kHz. Since we are considering the behavior of a PC flat lens immersed in water, we also illustrate in this figure

the dispersion curve of water (dashed lines). This dispersion curve describes a cone in reciprocal space and intercepts the second pass band, in which the group velocity is negative, at the frequencies of 543.5 ±1.6 kHz and 544.0 ±1.6 kHz in the ΓM and ΓK directions, respectively. This result shows that the equifrequency contour (EFC) of the PC is circular at this frequency (anisotropy is below 1%) and matches that of the water, in agreement with Ref. 8. This property means that in the case of a flat interface between water and the PC, all incident angles of waves originating from the water will undergo negative refraction at this frequency with an effective index of −1 upon propagation through the crystal. The EFC matching frequency of 544 kHz is consistent with that reported in Ref. 9 within the numerical accuracy of the FDTD band-structure calculation. All frequencies below 544 kHz in the second band will exhibit the so-called all angle negative refraction (AANR).

Figure 1(c) shows the band structure in the direction parallel to the face of the finite slab of PC in water consisting of six layers of rods. The inset depicts the supercell used in the FDTD calculations in which the material on the right represents water while the system on the left shows the PC consisting of a triangular lattice of steel cylinders immersed in methanol. The system is taken to be infinitely long in the vertical direction by imposing periodic boundary conditions on both top and bottom boundaries, while the thickness is taken to be that of the supercell. It is important to note that for this reason there exists a greater number of bands in the finite-thickness crystal band structure than in the infinite crystal band structure. In Fig. 1(c), the straight line represents the dispersion curve of water. It is important to note that modes which fall above the water line are propagative modes in the water-lens system while those which fall below are the modes bound to the PC slab. These modes have evanescent character in the direction perpendicular to the face of the PC, and are propagative in the direction parallel to the water-lens interface.

To study the focusing properties of the lens, we use a PC slab of 31 rods along its width and six rods along its thickness (i.e., a six-layer crystal with 31 rods per layer). Following Sukhovich *et al.*,[9] we use a line source (0.55 mm wide) running parallel to the principal axis of the steel cylinders with an operating frequency of $\nu = 530$ kHz. The value of the operating frequency, found to give the best experimental resolution of the focal spot, will be discussed in Sec. V A. FDTD mesh points belonging to the source emit a sinusoidal displacement at frequency ν, with components parallel and perpendicular to the surface of the lens. We investigate the imaging property of the lens in the form of a contour map of the field of the time-averaged absolute value of the pressure. Simulated results of the average of the absolute value of the pressure over one cycle are shown in Fig. 1(d), in which the source is located at a distance of 0.1 mm from the surface of the center cylinder on the input (left) side of the crystal. This configuration will be referred to as the "standard configuration" in subsequent sections. It is important to note that the chosen source width is smaller than the wavelength in water at the operating frequency, making it suitable for the investigation of super-resolution properties of the PC system. It can be seen in Fig. 1(d) that an image exists on the right

side of the crystal. This image is also accompanied by lobes of high pressure that decay rapidly with distance from the surface of the crystal. We define the resolution as the half-width of the pressure peak corresponding to the image. This value is determined by first locating the maximum amplitude of the image in the x_1-x_3 plane, as this corresponds to its center point, taking a vertical cut (parallel to the x_1 axis) through this point, and then fitting the data by a $\text{sinc}(2\pi x/\Delta)$ function. The half-width $\Delta/2$ is taken to be the distance from the central peak to the first minimum. The resolution for this system is found to be 0.34λ, where $\lambda = 2.81$ mm is the sound wavelength in water at the operating frequency. This result was confirmed experimentally in Ref. 9 and is significantly less than the value of 0.5λ that corresponds to the Rayleigh diffraction limit, demonstrating that the PC flat lens achieves super-resolution.

B. Experimental setup

Complementary experimental results are presented in this paper using the same measurement scheme as in Ref. 9. The two-dimensional (2D) PC used was made of 1.02 mm diameter stainless-steel rods arranged in a triangular lattice with lattice parameter of $a = 1.27$ mm. The surface of the crystal was covered by a very thin (0.01 mm) plastic film and the crystal was filled with methanol. A rectangular lens was constructed from six layers of rods, with 60 rods per layer, stacked in the ΓM direction of the BZ, i.e., with the base of the triangular cell parallel to the surface. The experiments were conducted in a water tank. The ultrasound source was a narrow subwavelength piezoelectric strip, 0.55 mm wide and 35 mm long, oriented with its long axis parallel to the steel rods; it was therefore an excellent approximation to a 2D point source. The spatiotemporal distribution of the acoustic field on the output side of the lens was detected with a miniature 0.40 mm diameter hydrophone mounted on a motorized stage, which allowed the field to be scanned in a rectangular grid pattern. This setup ensures that the widths of the source and detector are smaller than the wavelength in water ($\lambda = 2.81$ mm) at the frequency of operation (530 kHz). The lateral resolution of the focal spot is measured from the measured pressure field using the same method as described for FDTD results.

III. ORIGIN OF SUPER-RESOLUTION

To illustrate the phenomenon of focusing by a flat lens as well as of super-resolution, we propose to describe them, in the case of a doubly negative material, using a Green's function formalism.[20] Green's functions are particularly well adapted to the problem of imaging a point source, as they represent the response (here acoustic) of a medium, possibly inhomogeneous, to a point source stimulus. We consider a continuum model of a lens made of a negative index material infinite slab (medium 1) immersed in a fluid (medium 2) (Fig. 2). For a homogeneous flat lens, the acoustic Green's function can be expressed as a two-dimensional spatial Fourier transform in the plane parallel to the water-lens interface:

$$G\left(\vec{x},\vec{x}'\right) = \int \frac{d^2\vec{k}_{/\!/}}{(2\pi)^2} e^{i\vec{k}_{/\!/}(\vec{x}_{/\!/}-\vec{x}'_{/\!/})} g(k_{/\!/},x_3,x_3'), \quad (1)$$
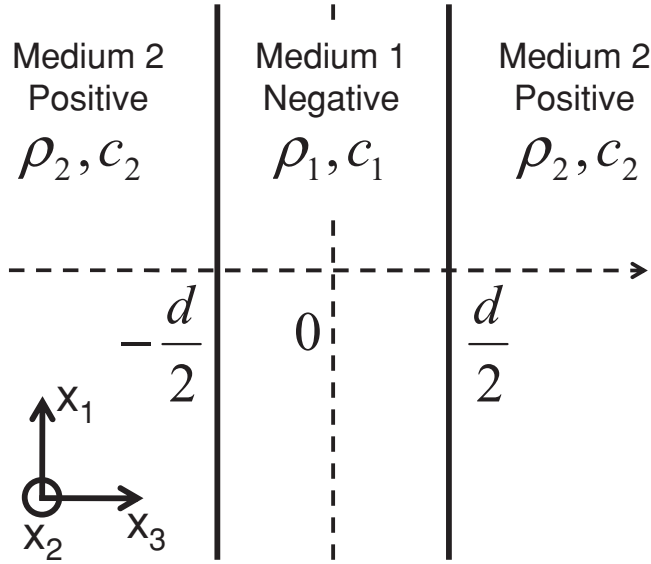
FIG. 2. Schematic representation of a flat lens consisting of a homogeneous composite medium (medium 1) immersed in water (medium 2).

where $\vec{k}_{//}$ and $\vec{x}_{//}$ are the components of the wave vector and position vector parallel to the (x_1, x_2) plane. This function describes the field generated at $\vec{x}$ by a point source located at $\vec{x}'$. For the composite medium composed of the flat lens (medium 1) of thickness d (with faces centered on $-d/2$ and $d/2$) immersed between two semi-infinite media 2, the Fourier transform of the Green's function, $g(k_{//}, x_3, x_3')$ can be expressed by the following equation:[20]

$$g(k_{//}, x_3, x_3')$$
$$= \frac{2\rho_1 c_1^2 \alpha_1 e^{-\alpha_2(x_3 - x_3' - d)}}{\left(\rho_1 c_1^2 \alpha_1 + \rho_2 c_2^2 \alpha_2\right)^2 e^{\alpha_1 d} - \left(\rho_1 c_1^2 \alpha_1 - \rho_2 c_2^2 \alpha_2\right)^2 e^{-\alpha_1 d}}$$
$$\text{for} \quad x_3' < -d/2 \text{ and } x_3 > d/2. \qquad (2)$$

Here, the subscripts 1 and 2 correspond to the two media and ρ denotes the density, c the phase velocity of sound, and $\alpha = -ik_3$, k_3 is the component of the wave vector perpendicular to the interface between medium 1 and medium 2. For the sake of analytical simplicity, Eq. (2) was obtained by treating both media as fluids, which is correct for medium 2 and reasonable for medium 1 since the matrix of the PC is fluid. We also note that the zeros of the denominator in Eq. (2) correspond to all propagating and bound modes of the system. Medium 2 is taken to exhibit a positive index of refraction with

$$k_3^{(2)} = i\sqrt{k_{//}^2 - \frac{\omega^2}{c_2^2}} \quad \text{if} \quad \omega \leqslant k_{//} c_2,$$
$$k_3^{(2)} = \sqrt{\frac{\omega^2}{c_2^2} - k_{//}^2} \quad \text{if} \quad \omega \geqslant k_{//} c_2. \qquad (3)$$

The condition in the first line of Eq. (3) describes evanescent waves (pure imaginary k_3) while the second condition describes propagating waves. By contrast, medium 1 consists

of a negative index material with

$$k_3^{(1)} = i\sqrt{k_{//}^2 - \frac{\omega^2}{c_1^2}} \quad \text{if} \quad \omega \leqslant k_{//} c_1,$$
$$k_3^{(1)} = -\sqrt{\frac{\omega^2}{c_1^2} - k_{//}^2} \quad \text{if} \quad \omega \geqslant k_{//} c_1. \qquad (4)$$

The choice of a negative sign in the case of propagating waves in Eq. (4) ensures causality as pointed out by Veselago.[21] Indeed, negative index materials take advantage of a negative group velocity at the operating frequency, i.e., the group velocity and wave vector point in opposite directions. Thus energy is transmitted forward by waves having a negative k_3. Consider that the point source operates at an angular frequency ω such that the equifrequency contours of the two media are equal in size (i.e., AANR is satisfied). Then, the phase velocities of both media take the value $c_1 = c_2 = c$. Therefore Eq. (1) can be rewritten as the sum of the integral over all propagating modes and all evanescent modes, giving the following expression:

$$G\left(\vec{x}, \vec{x}'\right) = \int_0^{k_{//}^2 = \omega^2/c^2} \frac{d^2 \vec{k}_{//}}{(2\pi)^2} e^{i\vec{k}_{//}(\vec{x}_{//} - \vec{x}_{//}')} g(k_{//}, x_3, x_3')$$
$$+ \int_{k_{//}^2 = \omega^2/c^2}^{k_m} \frac{d^2 \vec{k}_{//}}{(2\pi)^2} e^{i\vec{k}_{//}(\vec{x}_{//} - \vec{x}_{//}')} g(k_{//}, x_3, x_3'). \qquad (5)$$

The introduction of a cutoff k_m will be discussed in Sec. IV. To gain insight, we can further simplify the model with some loss of generality by assuming that $\rho_1 = -\rho_2 = -\rho \leqslant 0$. The negative sign of the density is due to the fact that medium 1 is a doubly negative material which means that both bulk modulus and density are negative. Through this simplification, one is able to obtain the Green's function for the composite medium of Fig. 2 in the form

$$g(k_{//}, x_{3,} x_3') = \frac{e^{-\alpha(x_3 - x_3' - 2d)}}{2\rho c^2 \alpha} \text{ for } x_3' \langle -d/2 \text{ and } x_3 \rangle d/2. \qquad (6)$$

If we assume that all evanescent modes contribute to the formation of the image (i.e., $k_m \to \infty$) and consider the response of this system to a point source located on the left side of medium 1 at a position $x_3' = -s - d/2$, where s is the distance from the source to the lens input surface, Eq. (5) can be integrated using the following formula:[22]

$$\sqrt{\frac{\pi}{2}} \frac{e^{-\alpha|\xi|}}{\alpha} = \frac{1}{\sqrt{2\pi}} \int_{-\infty}^{\infty} \frac{e^{i\xi x}}{\alpha^2 + x^2} dx. \qquad (7)$$

The resulting real-space Green's function takes the form

$$G(\vec{x}, \vec{x}_i) = \frac{e^{i(\omega/c)|\vec{x} - \vec{x}_i|}}{4\pi\rho c^2 |\vec{x} - \vec{x}_i|}, \text{ where } \vec{x}_i = \left(0, 0, \frac{d}{2} + d - s\right). \qquad (8)$$

This expression is that of a spherical wave originating at the point $\vec{x}_i$. It represents a perfectly reconstructed image of the point source. The homogeneity of medium 1 allowed the integration of all evanescent contributions in the derivation of Eq. (8) and is the crucial point that leads to perfect reconstruction. Denoting the distance of the image from the

lens output surface by i, the relationship between i and s is simply given by $i = d - s$.

This discussion, based on the assumption of a doubly negative homogeneous media, cannot apply to flat lenses composed of inhomogeneous periodic materials such as PCs. Indeed, in PCs, the mechanism leading to negative refraction is based on the Bragg scattering of waves in a crystalline structure whose constant is of the same order of magnitude as the wavelength. However, the fact that enhancement of resolution can occur due to the integration of evanescent components in Eq. (8) is still valid.

IV. LIMIT OF RESOLUTION

Superlensing requires amplification of the evanescent modes from the source during transmission through the lens.[1] In the case of photonic crystals, Luo *et al.*[13] have shown theoretically that coupling evanescent waves to a bound mode of the photonic crystal lens is a suitable mechanism to realize this amplification. In their scheme, the energy from nonpropagative components of the light emitted by the source excites the bound mode of the slab in a resonant manner, which may take a certain time to reach the steady-state regime depending on the $k_{//}$ component of the incident mode. The re-emitted evanescent waves can contribute to the image since their amplitude is restored through transmission. By this mechanism one can virtually build an image up to an arbitrary resolution provided all evanescent modes are amplified and a sufficient time is available to reach the steady-state regime for all evanescent modes. However, in a real situation the first condition is not realized, so the authors introduced a cutoff for $k_{//}$, which led to a method to calculate the maximum resolution for a photonic crystal flat lens. In this section, we consider a similar method in order to estimate the ultimate resolution one can achieve with our acoustic lens system.

First, it is apparent in the field pattern of Fig. 1(d) that super-resolution is associated with the intense excitation of acoustic modes bound to the lens (see Sec V C.). Theses modes, near the operating frequency, are bulk modes of the finite slab, not surface modes that decay rapidly inside the slab.

The discussion in Sec. III assumed a homogeneous negative index material and cannot be applied to PCs, which are inhomogeneous periodic materials. When considering PC flat lenses, it is not possible to enable all evanescent modes from the source to contribute to the reconstruction of the image. The upper bound of the integration is determined by the largest wave vector k_m parallel to the lens surface that is compatible with the periodicity of the PC in that same direction and that can be excited by the sound source.

Therefore to find the resolution limit, we must determine the maximum magnitude of the transverse wave vector of an incident evanescent wave that can excite a bound mode in the slab. This cutoff k_m is introduced as the upper bound of the second term of Eq. (5), which accounts for the reconstruction from evanescent components. In Fig. 3, the dispersion curves of the slab immersed in water are shown in the direction parallel to the lens surface. The dashed diagonal lines are the dispersion curves of acoustic waves in water and the dotted horizontal line represents the operating frequency. At this
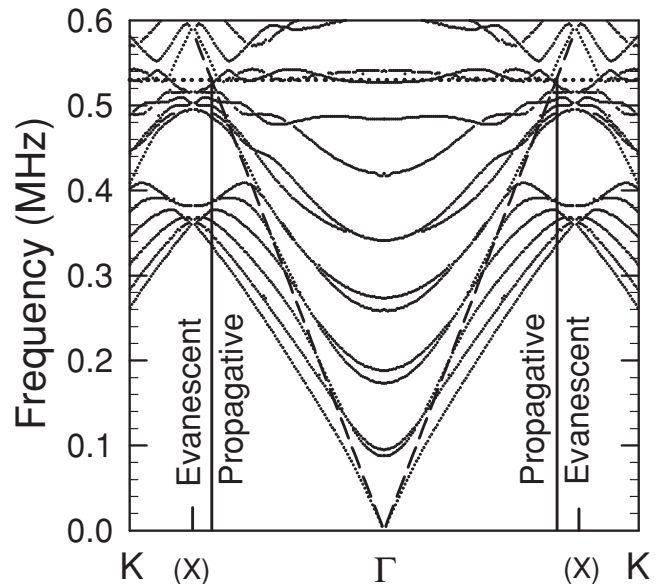

FIG. 3. Determination of the maximum wave vector contributing to the super-resolution. The FDTD band structure of the finite slab is plotted in the direction parallel to the lens surface for the range of wave vectors extending up to the edge of the Brillouin zone of the hexagonal lattice of the PC. Dashed lines represent dispersion relations of water. Modes that fall above these lines can propagate in water while those that fall below exhibit evanescent character. The dotted line depicts the operating frequency of the source. On the bottom axis, the X point of the (1D) surface Brillouin zone is indicated.

frequency, the wave vector components of the incident wave with $k_{//} < \omega/c$ can propagate in the crystal; they will form an image according to classical geometric acoustics. Components with $k_{//} > \omega/c$ will couple to the bound modes of the slab provided that these bound modes dispersion curves are in the vicinity of the operating frequency. In this way, the existence of many modes of the slab with nearly flat dispersion curves in the vicinity of the operating frequency is favorable for achieving super-resolution, as mentioned in Ref. 13. One might imagine that evanescent waves with transverse wave vector of any magnitude above ω/c could couple with bound modes. However, the modes that propagate through the thickness of the lens must resemble those of the infinite periodic PC. The symmetry of the waves inside the lens must therefore comply with the triangular symmetry of the PC. More precisely, the modes of the crystal are periodic in k space with a period equal to the width of the first 2D triangular Brillouin zone. This is the reason why the x axis of Fig. 3 has been extended up to the K point of the hexagonal lattice reciprocal space. If an incident wave has a wave vector above the first Brillouin zone boundary, then it will couple to a mode having a wave vector that can be written as $\vec{k}'_{//} = \vec{k}_{//} + \vec{G}$ where $\vec{G}$ is a reciprocal lattice vector and $\vec{k}'$ lies in the first Brillouin zone. In our case, since the first Brillouin zone of a triangular lattice extends from $-4\pi/3a$ to $4\pi/3a$ in the ΓK direction (parallel to the lens surface), the information carried by incident evanescent

waves with transverse wave vector components,

$$||k_{//}|| > k_m = \frac{4\pi}{3a}, \tag{9}$$

is lost and will not contribute to the formation of the image.

Then, as suggested by Luo *et al.*, the width of the image can be estimated by assuming that there is complete transmission from the source to the image for $k_{//} \leqslant k_m$ and zero transmission for $k_{//} > k_m$. This leads to a transverse image profile given by a sinc function with width $\Delta = 2\pi/k_m$, defined as the distance between first zeros of the sinc function. With this definition, one finds that the best possible image resolution is $\frac{\Delta}{2} = \frac{3a}{4}$. Applying this estimate to our PC with $a = 1.27$ mm, and a wavelength in water at 530 kHz of 2.81 mm, the minimum feature size that would be resolvable with this system is 0.34λ. This estimate matches our results very well for the best resolution found in our system (0.34λ), presented in Sec. II, and with experiment (0.37λ).

V. EFFECTS OF OPERATIONAL AND GEOMETRICAL FACTORS

In this section, we explore the effects of several factors on the image resolution of the PC flat lens. These factors include operational factors such as the source frequency and the position of the source and geometrical factors such as width and thickness of the lens. By exploring modifications to the system, we aim to shed light on the parameters that have the greatest impact on the imaging capabilities of the PC lens and understand their effects as they deviate from the best operating conditions.

A. Operating frequency

In Sec. II, the operating frequency of the source was chosen to be 530 kHz, as in Ref. 9. Here we focus on the effects of tuning the operating frequency in the 510–560 kHz range, while all other factors are kept the same as described in Sec. II. The lateral image resolution and distance of the focus from the exit surface of the lens obtained from the FDTD simulation and from experiments are plotted in Fig. 4. Experimental and simulation results are in reasonable agreement from 523 to 560 kHz. The experimental values are slightly higher than the computed values, with a difference not exceeding 0.05λ. Experiments exhibit an optimum resolution (0.37λ) at 530 kHz. As the frequency increases, the image width increases up to the Rayleigh value (0.5λ). There is very good overall agreement in the observed values of the resolution and in the change in focal distance with frequency. However, in the experiments, the images are found to form nearer the crystal than in these simulations, likely reflecting the difference in the frequencies at which perfect equifrequency contour matching is found (544 kHz in the current simulations and 550 kHz in the experiments). Indeed, if one compares the experimental and simulated results, for both the resolution and image distance, at frequencies that differ from the corresponding EFC matching frequencies by the same amounts, the agreement is remarkably close.

We now propose an interpretation of these results based on both matching of the AANR condition and excitation of bound modes of the PC. The scheme in Fig. 5 depicts the
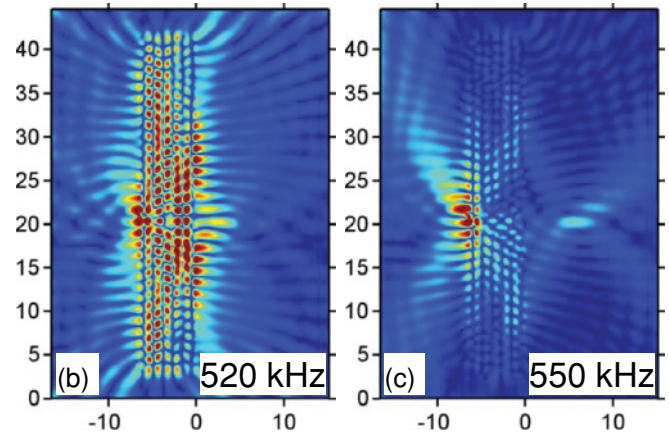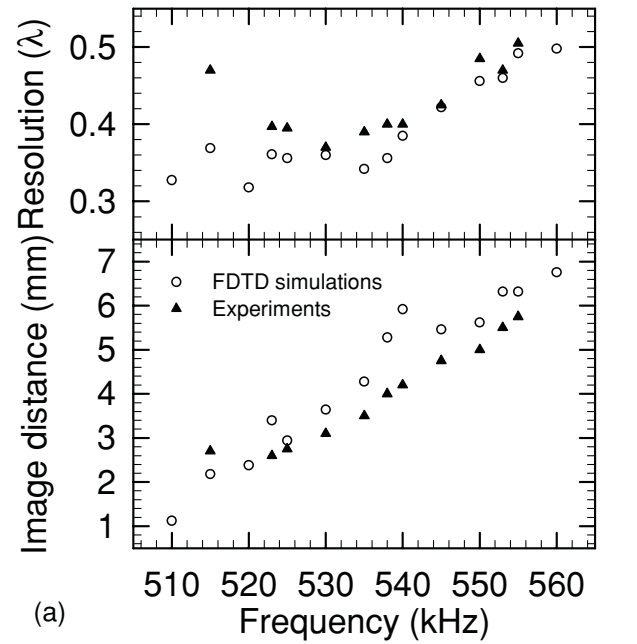

FIG. 4. (Color online) Effects of the operating frequency. (a) Lateral resolution and distance of the image as a function of the operating frequency. Results from experiments (triangles) are compared to FDTD simulation (circles). Pressure fields at 520 kHz (b) and 550 kHz (c).

EFC in water and in the PC for different frequencies as circles of different diameters. First, we observe that if the frequency of the source is tuned lower than 544 kHz, super-resolution is achieved with a resolution below 0.39λ (see also Fig. 4). Since the operating frequency is lower than 544 kHz, the equifrequency contour of water is a smaller circle than the EFC inside the crystal [see Fig. 1(b)]. Thus all components of the incident wave vectors corresponding to propagating modes can be negatively refracted by the crystal, i.e., the AANR condition is satisfied. However, the mismatch of the equifrequency contours diameters leads to a negative effective index of refraction with magnitude greater than 1, causing the different components from the source to focus at different places. On the other hand, operating frequencies well below 544 kHz are close to the flat bands of bound modes in the PC slab, allowing for efficient excitation by the evanescent waves from the source (Fig. 3). These modes are depicted as a gray region on the EFC of the slab in Fig. 5. Thus the
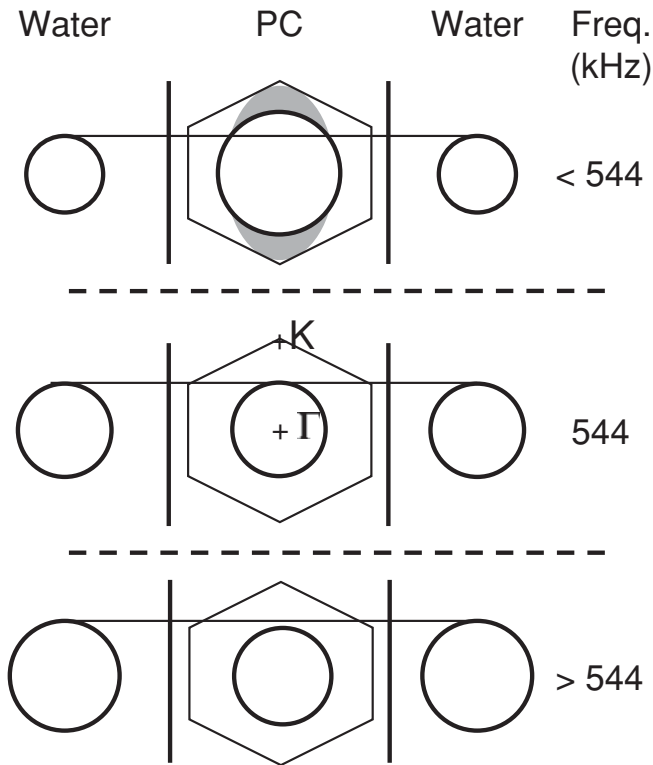
FIG. 5. Schematic representation of the transmission through the PC lens based on the equifrequency contours shapes. The equifrequency contour of the PC lens is represented as a circle inside the first Brillouin zone of the hexagonal infinite crystal. The gray areas illustrate the existence of bound modes with frequency very close to the operating frequency.

gain from the amplification of evanescent modes is retained and super-resolution is achieved. This excitation of bound modes of the PC lens at frequencies well below 544 kHz is consistent with the intense pressure field observed inside the PC in Fig. 4(b). At the frequency of 544 kHz the EFC of water and the PC have the same diameter resulting in an effective index of −1. This condition implies a perfect focusing of all propagating components of the source into a single focal point. However, Fig. 3 shows that the flat bands of bound modes of the lens are now well below the operating frequency, which means that coupling with these modes and amplification of the evanescent waves during transmission is now inefficient. The experimental optimum of the lateral resolution at 530 kHz occurs between the bound mode frequencies (∼510 kHz) and the perfect matching of the equifrequency contours (544 kHz). These results confirm the importance of the design of the PC superlens with respect to two conditions. First, one has to meet the AANR condition, which requires that the PC be a negative refraction medium with a circular EFC matching the EFC of the outside medium (water). Second, bound modes must exist in the PC whose frequencies are close to the operating frequency so that amplification of evanescent components may occur. The optimum frequency is found as the best compromise between those two parameters.

Finally, if we consider an operating frequency above 544 kHz, the EFC of water has now a greater diameter than the

EFC of the PC, resulting in an effective index with magnitude lower than unity. In that case, the AANR condition is not matched and a part of the propagating components experience total reflection at the water-lens interface. The resolution still worsens and reaches 0.5λ at 555 kHz. Figure 4(c) shows the pressure field at 550 kHz. The poor excitation of the PC confirms the fact that bound modes cannot be excited because their frequency is too low compared to the excitation frequency. In terms of the image distance, according to acoustic ray tracing, the focal point changes as a function of the acoustical index mismatch. Here, since the magnitude of the effective acoustic index of the PC decreases as the frequency increases, the image appears farther from the lens exit surface for higher frequencies. This trend, confirmed by experiments as well as simulations [see Fig. 4(a)] shows the high sensitivity of the image location to changes in frequency. Here, tuning the frequency from 523 to 555 kHz shifts the image from 2.6 to 5.75 mm.

B. Location of the source in the direction parallel to the lens

Here, we consider the effects of the position of the source with respect to the PC surface. In order for super-resolution to take place, evanescent wave components emitted from the source must couple to bound slab modes in the PC, resulting in amplification and re-emission to form an image. Thus the PC must lie in the near field of the point source. In these conditions the distance from source to lens and the period of the PC (lattice constant) are comparable in magnitude, so that the local structure of the PC bound modes near the crystal surface affects the focusing process. To gain further understanding of this process we simulated the case of a source facing the gap midway between two cylinders of the PC, all other parameters being kept the same as the standard configuration. In this case, the resolution falls to 0.54λ. Similar results were found in the experiments. For example, moving the source parallel to the surface from the position opposite a cylinder (best resolution) by only a quarter of its diameter caused the image resolution to degrade from 0.37λ to 0.47λ. In another experiment, moving the source to a position midway between the cylinders caused the image width to increase by 55%, similar to the degradation in image quality found in the simulations. Although the AANR condition is satisfied, the bound modes are not excited when the source is facing the gap between the cylinders. This result can be understood by noting that the source is now located at a maximum of the pressure field of the bound modes (i.e., a minimum of the displacement field since pressure is proportional to the gradient of displacement). Indeed, when super-resolution is achieved, the amplitude of the bound modes dominates the pressure field because of resonant amplification. For that reason, looking at Fig. 1(d) gives an idea of the pressure field and indirectly the displacement field of these modes. The pressure exhibits lobes of maximum amplitude between cylinders and consequently the displacement amplitude would show maxima in front of each cylinder and nodes between them. Placing the source at any of the nodes of the displacement field prevents evanescent waves from coupling efficiently with the bound modes.

C. Distance from the source to the lens

We now consider the effects of changing the distance from the source to the lens in the direction normal to the lens surface, along x_3. One expects two different effects. First, if the lens is placed far enough beyond the near field of the source, super-resolution should no longer be observed. Second, according to both acoustic ray tracing and the Green's functions model presented in Sec. III, the distance i of the image from the lens output surface should decrease as the distance of the source s from the lens input surface is increased, being given when the equifrequency contours are perfectly matched by $i = d - s$. In Fig. 6(a), the lateral resolution and distance of the image are plotted as a function of the source distance. The dashed horizontal lines represent the Rayleigh diffraction limit (0.5λ)
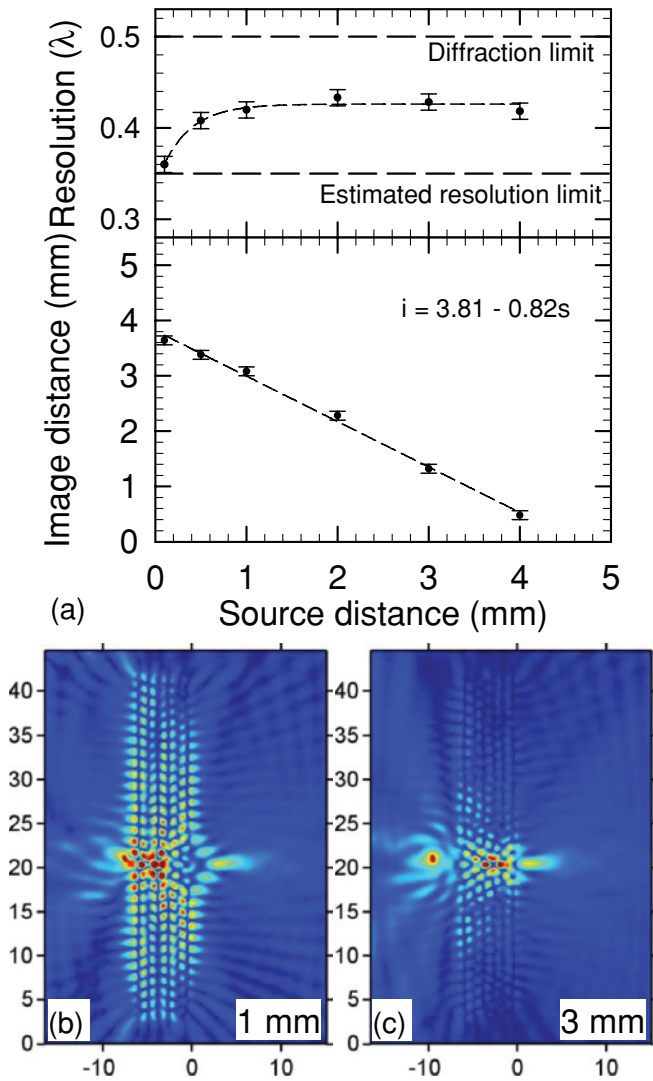

(a)

FIG. 6. (Color online) Effects of the source distance. (a) Plot of the resolution and image distance as a function of the source distance. As the distance increases, excitation of the modes bound to the PC is less efficient, resulting in a loss of resolution. (b) Contour maps of the time-averaged absolute value of the pressure with the source positioned 1 mm (b) and 3 mm (c) away from the incident face of the PC lens.

and the estimated maximum resolution limit (0.34λ) calculated in Sec. IV.

Figures 6(b) and 6(c) show the time-averaged absolute pressure field in the standard PC system for distances of 1 and 3 mm from the source to the lens surface. One can see in Fig. 6(b) that the bound modes are clearly excited when the source is in close proximity to the face of the lens, corresponding to a high pressure field across the entire length of the PC. At this range of distances, the resolution is close to the maximum limit calculated before. One should also note that the bound modes have large amplitude near the lens surface, which is in accordance with the resonant character of the amplification of evanescent modes. Figure 6(c) shows that as the distance between the source and the face of the lens is increased, excitation of the bound modes is less and less effective and the resolution decreases. For this range of image distances, the resolution remains smaller than the Rayleigh diffraction limit. The fact that this limit is not reached is related to the close distances which are considered here, which range from λ/28 to 1.4λ. Thus the lens is always in the near field of the source for the studied range. One expects that for larger distances the resolution will reach the Rayleigh diffraction limit, accompanied by loss of super-resolution. However, for a source placed farther than d, acoustic rays tracing predicts that no focusing occurs and the image takes on a virtual character. We have tested this point and indeed for a source placed far from the lens we find a diverging beam on the opposite side of the lens. Thus to observe the complete loss of super-resolution would require a significantly thicker lens and a larger source distance, conditions that were not possible with our computation capabilities. In Sec. III, a Green's function model was used to show that if all evanescent and propagative modes are contributing then the image is perfectly reconstructed as a point source at a distance $d - s$ from the exit face of the lens. This is the exact position that geometric rays tracing predicts if the two media have opposite refraction indices. This linear behavior would also be expected if there was an impedance mismatch between the lens and the embedding medium or if the media had uniaxial anisotropy in the x_3 direction.[3] To verify the relationship between source and focal distances we plot the distance of the image from the lens exit surface as a function of source distance from the incident surface [see Fig. 6(a)]. The simulation results fit a linear relation with a slope of −0.82. However, the intercept of this curve differs from the predicted value of $d = 6.52$ mm (the thickness of the lens). We have shown in Sec. V A that the position of the image is very sensitive to the frequency because the operating frequency defines the effective index of the PC. If n is the effective index of the PC relative to water, then the focus position for a source placed very close to the lens is d/|n| Since the operating frequency is 530 kHz, i.e. not exactly the frequency for which $n = -1$, the magnitude of the refractive index is greater than 1. Thus the fact that the intercept on Fig. 6(a) is lower than the lens thickness d could be explained in terms of refractive index mismatch between the two media. We find $n = 1.07$ for the operating frequency. However, this value alone is insufficient to explain completely the discrepancy. This discrepancy is therefore most probably due to the fact that the lens is made from a PC and is therefore not a homogeneous negative medium as assumed in

the Green's functions-based model. Indeed, the need for considering a homogeneous medium with an effective thickness has arisen in the case of homogenization of a metamaterial slab.[23]

D. Geometry of the PC lens

In addition to the operating factors discussed in the previous sections, it is also of interest to examine the effects of the thickness and width of the PC lens. The width of the lens is measured along x_1 by the number of rod inclusions in each layer parallel to the surface. We simulated lenses of 15, 31, and 61 rods per layer in crystals with our standard thickness of six layers, all other parameters being constant. We found that the behavior of the lens with 61 rods per layer does not differ from that of the standard case. More specifically, the position of the image and resolution as a function of the position of the source [Fig. 6(a)] gave the same results. By contrast, the results for
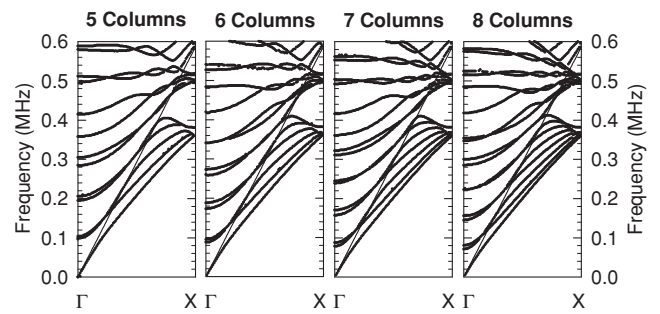
FIG. 8. FDTD band structure calculations in the direction parallel to the face of the PC for lenses with 5, 6, 7, and 8 layers. Whatever the number of layers, bound modes (flat curves) are always present at the zone edge with frequencies very close to the operating frequency of 530 kHz.

the narrower lens (i.e., 15 rods per layer) were significantly different. We attribute this observation to the lens's small aspect ratio (2.5), which was too small to avoid significant distortions. For lenses wider than 31 rods, the aspect ratio is greater than 5 and does not affect the results.

The thickness of the lens was varied by changing the number of layers of cylindrical inclusions [columns in diagram of Fig. 1(a)]. We simulated lenses having a thickness of 4, 5, 6, 7, and 8 layers for the case with a width of 31 rods per layer. The distance from the source to the surface was maintained at 0.1 mm as in the standard configuration. Figure 7(a) summarizes the results for the resolution and image distance. We note that for all lenses the resolution does not change to within the range of measurement error. This fact indicates that, in these cases, excitation of the bound modes is achieved as suggested by the intense pressure fields observed inside the PC lenses [Figs. 7(b) and 7(c)]. This was confirmed by conducting a series of band structure calculations in the direction of $k_{//}$ for each lens thickness (Fig. 8). The PC lenses exhibit bound modes whatever the thickness studied. The frequencies of the bound modes that are responsible for super-resolution do not vary significantly as the thickness changes. There is a slight shift in frequency near the Γ point but no significant shift away from our operating frequency at the X point. To further elucidate this point, we consider as a toy model the Lamb modes in an infinitely long plate with finite thickness. For such a plate it is found that the behavior of the frequency of the Lamb modes as a function of thickness is dominated by the magnitude of the wave vector for the lower order modes.[24] This is in agreement with observed behavior of our band structure calculations for different thicknesses of the PC. The number of bound modes increases as expected with the number of layers of inclusions.

The distance of the image from the crystal surface increases linearly with the thickness of the lens. However, the fitted value of this slope is not 1, as expected in the case of a homogeneous negative medium, but 0.83. We have seen earlier in Sec. V D that a lens made of an effective homogeneous medium may not have the thickness of the actual phononic lens. The discrepancy between the slope of 0.83 compared to 1 indicates the thickness mismatch between effective homogeneous slabs and phononic crystal slabs.[23]
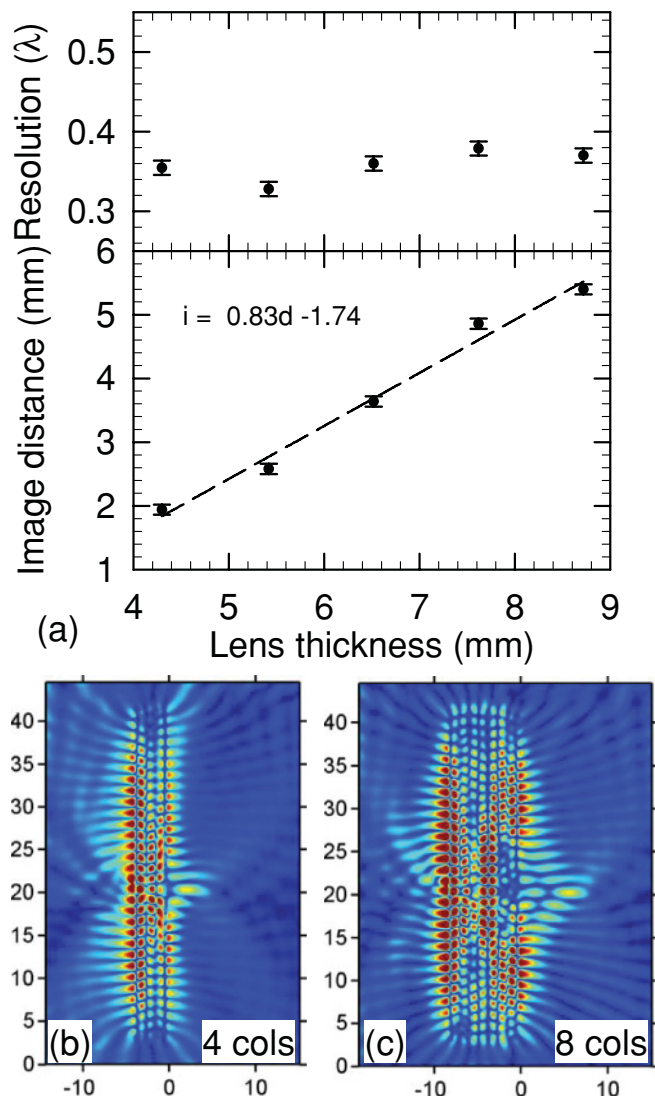

FIG. 7. (Color online) Effects of the number of layers. (a) Lateral resolution and distance of the image as a function of the number of layers. Pressure fields are drawn for the four layers (b) and eight layers (c) lenses.
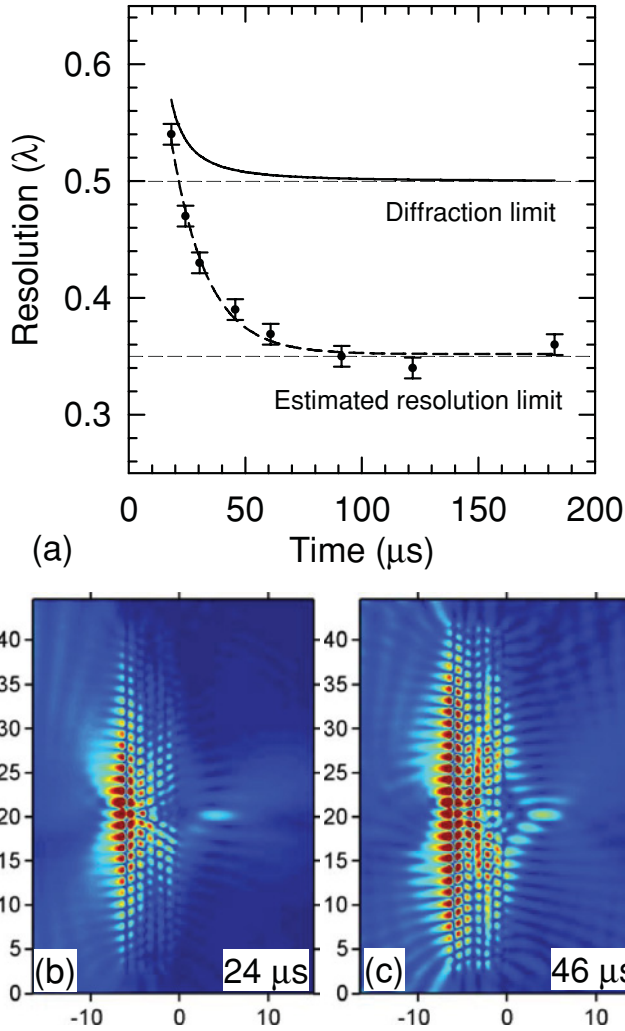
FIG. 9. (Color online) (a) Time evolution of the lateral resolution of the image in the standard configuration. The dashed line is an exponential fit to the data points, determined from FDTD simulations. The solid line is the lateral resolution of the half-width ($\Delta_p/2$) as a function of time, as estimated using a simple ray tracing model involving only propagating modes (see text). (b) Pressure fields after 24 μs and (c) after 46 μs of propagation.

E. Resolution as a function of time

As mentioned in Sec. IV, the lens requires sufficient time to establish a steady state image. To investigate the temporal evolution of the image we measured the lateral resolution obtained at various delays after the start of the simulation. Figure 9(a) (shows the resolution as a function of time for the standard configuration. The half-width of the image appears to decrease exponentially from values above the Rayleigh limit at short times to super-resolution after long times. In this same figure we also plot an estimate of the resolution considering only propagating modes and ray tracing arguments for a homogeneous flat lens with perfect equifrequency contour matching to the surrounding medium. The half-width of the image in this case is simply given by

$$\frac{\Delta_p}{2} = \frac{\pi}{k_{//\max}(t)} = \frac{0.5\lambda}{\sqrt{1 - \left(\frac{2d}{ct}\right)^2}}, \tag{10}$$

where t is time and c is the speed of sound in water. This relation is plotted as a solid line in the figure. This line suggests that it takes approximately 20 μs to achieve 90% of the Rayleigh diffraction limit. The simulated data indicate that more time is needed to achieve super-resolution. One needs approximately 60 μs to achieve 90% of the ultimate resolution. The additional time is necessary to excite the lens bound modes. This is clearly seen in Figs. 9(b) and 9(c) where the bound modes propagate along the length of the lens until complete excitation is achieved.

VI. CONCLUSIONS

As a followup to a recent report demonstrating experimental and theoretical subwavelength imaging in a phononic crystal flat lens,[9] we have provided a thorough analysis of the physical requirements for achieving superlensing. For this, we employed a combination of analytical and numerical methods, supported by experimental results. We described analytically the resolution of an image formed from negatively refracting material using a Green's functions formalism, providing an expression for a perfectly reconstructed image. We have shown that perfect reconstruction requires that all propagative and evanescent components of the source contribute to the formation of the image. Using the FDTD method we showed that for a phononic crystal, the evanescent components of a source can be amplified by excitation of bound modes of the flat lens. We have extended the work of Luo *et al.*[13] on photonic crystal superlensing to predict the ultimate resolution of acoustical superlenses composed of triangular arrays of cylindrical inclusions in a matrix. The predicted resolution is limited by the symmetry of the crystal and is in excellent accord with the ultimate resolution calculated with FDTD, as well as with the reported experimental value.[9] Our discussion of subwavelength imaging was further extended by exploring the effects on super-resolution of geometrical and operational factors, such as source position, frequency, PC dimensions, and propagation time. More specifically, these effects were analyzed in the context of the interplay between AANR and sufficient coupling of evanescent source components to bound modes of the crystal. Because of its relevance to experiments, further analysis of subwavelength imaging in a phononic crystal flat lens is planned to thoroughly evaluate the detrimental effects of positional randomness of the steel rods, as well as other imperfections, on both the focal point and resolution. Indeed, since negative refraction relies on multiple scattering, it is expected to be highly sensitive to the regularity of the PC, as suggested by previous numerical and experimental results.[9] In summary, the work reported in this paper provides a detailed analysis of the physical principles underlying subwavelength imaging using phononic crystals, and will serve as a guide for the design of new phononic crystal lenses with optimum resolution capabilities.

*jrobilla@email.arizona.edu

†Géosciences Azur, 2 quai de la Darse, BP 48-06235, Villefranche-sur-Mer, France.

[1] J. B. Pendry, Phys. Rev. Lett. **85**, 3966 (2000).

[2] J. Li, K. H. Fung, Z. Y. Liu, P. Sheng, and C. T. Chan, in *Physics of Negative Refraction and Negative Index Materials*, Springer Series in Materials Science, Vol. 98, Chap. 8 (Springer, Berlin, Heidelberg, 2007).

[3] P. Sheng, J. Mei, Z. Liu, and W. Wen, Physica B **394**, 256 (2007).

[4] S. Yang, J. H. Page, Z. Liu, M. L. Cowan, C. T. Chan, and P. Sheng, Phys. Rev. Lett. **93**, 024301 (2004).

[5] J. H. Page, A. Sukhovich, S. Yang, M. L. Cowan, F. Van Der Biest, A. Tourin, M. Fink, Z. Liu, C. T. Chan, and P. Sheng, Phys. Status Solidi B **241**, 3454 (2004).

[6] K. Imamura and S. Tamura, Phys. Rev. B **70**, 174308 (2004).

[7] M. Ke, Z. Liu, Z. Cheng, J. Li, P. Peng, and J. Shi, Solid State Commun. **142**, 177 (2007).

[8] A. Sukhovich, L. Jing, and J. H. Page, Phys. Rev. B **77**, 014301 (2008).

[9] A. Sukhovich, B. Merheb, K. Muralidharan, J. O. Vasseur, Y. Pennec, P. A. Deymier, and J. H. Page, Phys. Rev. Lett. **102**, 154301 (2009).

[10] Z. He, X. Li, J. Mei, and Z. Liu, J. Appl. Phys. **106**, 026105 (2009).

[11] F. Liu, F. Cai, S. Peng, R. Hao, M. Ke, and Z. Liu, Phys. Rev. E **80**, 026603 (2009).

[12] P. Sheng, Nat. Mater. **8**, 928 (2009).

[13] C. Luo, S. G. Johnson, J. D. Joannopoulos, and J. B. Pendry, Phys. Rev. B **68**, 045115 (2003).

[14] M. Torres, F. R. Montero de Espinosa, and J. L. Aragón, Phys. Rev. Lett. **86**, 4282 (2001).

[15] D. Garcia-Pablos, M. Sigalas, F. R. Montero de Espinosa, M. Torres, M. Kafesaki, and N. Garcia, Phys. Rev. Lett. **84**, 4349 (2000).

[16] T. Miyashita and C. Inoue, Jpn. J. Appl. Phys. **40**, 3488 (2001).

[17] Ph. Lambin, A. Khelif, J. O. Vasseur, L. Dobrzynski, and B. Djafari-Rouhani, Phys. Rev. E **63**, 066605 (2001).

[18] M. Sigalas and N. Garcia, J. Appl. Phys. **87**, 3122 (2000).

[19] G. Mur, IEEE Trans. Electromagn. Compat. **EMC-23**, 377 (1981).

[20] P. A. Deymier, B. Merheb, J. O. Vasseur, A. Sukhovich, and J. H. Page, RMXFAT **54**, 74 (2008).

[21] V. G. Veselago, Sov. Phys. Usp. **10**, 509 (1968).

[22] I. S. Gradshteyn and I. M. Ryzhik, *Tables of Integrals, Series, and Products*, 5th ed. (Academic, London, 1965), p. 359.

[23] V. Fokin, M. Ambati, C. Sun, and X. Zhang, Phys. Rev. B **76**, 144302 (2007).

[24] K. F. Graff, *Wave Motion in Elastic Solids* (Dover, New York, 1991).